Polarization effects in electron scattering from ion cores in solids

G. Beni, P. A. Lee, and P. M. Platzman
Bell Laboratories, Murray Hill, New Jersey 07974
(Received 10 February 1976)

In current theories of x-ray absorption fine structure (EXAFS) and of low-energy electron diffraction, the elastic scattering of the photoelectrons from the ion cores in a solid is treated as the scattering from a static potential. We consider the effects of virtual excitation processes and discuss under which circumstances the polarization of the ion cores by the scattered electron are important. A complex energy-dependent optical potential is derived and a set of complex phase shifts are calculated with parameters appropriate for copper metal. Implications for the theory of EXAFS are discussed.

I. INTRODUCTION

Recently considerable effort has gone into the calculation of the properties of extended x-ray absorption fine structure[1-3] (EXAFS) and low-energy electron diffraction (LEED) spectra.[4] One of the central features of both of these calculations is an analysis of the single-electron atomic scattering problem. This scattering is typically characterized by a set of energy-dependent phase shifts. Until now these phase shifts have been calculated in one of two approximations: (i) By using an atomic potential[5] based on some form of Hartree-Fock-Slater approximation (e.g., the self-consistent potential used in band-structure calculations). (ii) A self-consistent Hartree-Fock scattering[6] theory using ground-state atomic wave functions as input.[4]

A feature of all of these calculations to date, is the use of a *constant* (in space and energy) complex potential to describe damping.[7] Such an assumption should be valid if the main source of damping is plasmon excitation. However, in transition and noble metals the occupied $3d$ states can constitute a major source of damping when the incident electrons have energies above the excitation threshold for d electrons. Since these d electrons are relatively localized within the muffin-tin sphere we might expect that the excitations of these electrons would lead to a nonuniform damping mechanism.

On quite general grounds we expect nonuniform damping to lead to important effects in the elastic scattering channel. This is easy to see of we remember that the scattering cross section of an electron with momentum k_i from any spherical localized object is quite generally given by[8]

$$\frac{d\sigma}{d\Omega}=\frac{1}{4k_i^2}\left|\sum_l (2l+1)(e^{2i\delta_l}-1)P_l(\cos\theta)\right|^2. \qquad (1)$$

When there is no absorption the δ_l are real and the maximum scattering cross section for any partial wave occurs when $\delta_l=\frac{1}{2}\pi$, i.e., $|\exp(2i\delta_l)-1|^2=4$. However it is quite clear from Eq. (1) that if δ_l has a large imaginary part (strong nonuniform absorption), then the elastic scattering in the lth partial wave approaches $\frac{1}{4}$ of the unitarity limit, i.e., $|\exp(2i\delta_l)-1|^2=1$. The physics of such strong diffraction scattering in this case is simple. The complete absorption of any partial wave implies that we are missing this wave when we want to reconstruct the incoming plane wave. This must of necessity lead to a large elastic scattering.

In a recent experiment[9] involving electron scattering by atomic copper in the 100-eV range, large inelastic scattering has been observed, which in turn greatly enhances the elastic scattering, particularly near the forward direction. While the large magnitude of the effect remains a puzzle it is clear that such effects are very important in electron-atom scattering. Of course when we go from an atom to a solid the valence levels broaden out to form bands. However, one expects that excitation of core levels or relatively localized states like the d bands in noble metals will have atomlike behavior. It is the purpose of this work to examine in detail the extent to which excitation of occupied electronic states in a solid lead to nonuniform damping. Having ascertained this we will then want to study the consequences of such nonuniform absorption as it applies to the elastic scattering of electrons in the several-100-eV range. Explicit calculations of the phase shifts for metallic copper will be carried out and the implication for the EXAFS spectrum in this material will be discussed. In particular we will reexamine the problem of the so-called fourth-shell anomaly.[2] In addition we will briefly, by means of numerical comparison, show how the differences between the Hartree-Fock (HF) and Hartree-Fock-Slater (HFS) calculations of electron phase shifts may be reconciled with the ideas presented here.

II. POLARIZATION PROCESSES

Consider the scattering of an electron with initial momentum k_i to a final state, characterized by a momentum k_f, by an atom. We will assume that the energy of the incident electron is sufficiently great so that we may neglect exchange effects. In this case the scattering amplitude may be written down as an infinite set of Born approximation scatterings. Such scattering events are shown schematically in Fig. 1. Here the single lines represent the free-electron propagator while the double solid lines labelled by the index n represent the atom with one-electron wave function $\varphi_n(r)$. The dashed lines characterize the Coulomb interactions between the high-energy electron and the atomic electrons together with the nucleus. It is this interaction which gives rise to the scattering.

The leading term Fig. 1(a) gives the usual Hartree result (throughout this paper we use atomic unit $e = m = \hbar = 1$)

$$f^{(1)}(\eta) = [\rho(\eta) - 1]/\eta^2 , \tag{2}$$

where

$$\rho(\eta) = \int e^{i\vec{\eta}\cdot\vec{r}} \varphi_0^2(r)\, d^3r ,$$

and $\vec{\eta} \equiv \vec{k}_f - \vec{k}_i$ is the momentum transfer. The second-order Born approximation is more complex and the process corresponding to Fig. 1(b) is of the form

$$f^{(2)}(\vec{\eta}) = \frac{2}{\pi^2} \sum_{n\neq 0} \int d^3q \, \frac{M_n^*(\vec{q} - \vec{\eta}) M_n(\vec{q})}{q^2 |\vec{q} - \vec{\eta}|^2 [q^2 + 2(\epsilon_n - \epsilon_0) + 2\vec{q}\cdot\vec{k}_i - i\delta]} . \tag{3}$$

The summation over n is a sum over the internal states of the atom with energy ϵ_n, and

$$M_n(\vec{q}) = \int d^3r \, \varphi_0^*(\vec{r}) e^{i\vec{q}\cdot\vec{r}} \varphi_n(\vec{r}) . \tag{4}$$

The term $n = 0$ in Eq. (3) has been dropped since it is simply the iteration of the lower Born approximation, Eq. (2). The effect of this term is properly accounted for by solving the Schrödinger equation with the Hartree potential. Unlike the contribution from the first Born approximation this second-order amplitude may be complex. Whenever an inelastic channel opens up, i.e., when the energy denominator in Eq. (3) can be zero we get an imaginary contribution.

At low incident energies k_i these inelastic channels are closed. At high energies the contributions from this second-order term and from all high-order terms are small relative to the leading term [Eq. (2)] due to the large size of the energy denominators which occur and to the large values of momentum transfer q which are required to satisfy the energy δ function. Thus, it is reasonable to expect that the inelastic processes will be most important in the intermediate energy range where the energy of the incoming electron is larger than but still comparable to the binding energy of the localized electrons. It turns out, as we will discuss in more detail for Cu that about one order of magnitude times the binding energy is a good estimate for the energy range involved.

In general, one cannot evaluate Eq. (3) without making some further approximations. However, it is possible to understand qualitatively how such a formal expression leads to a strongly enhanced forward scattering amplitude. Massey and Mohr[10] were the first to point out how the dynamic polarization of the atom, i.e., the excited internal intermediate state induced by the electron could result in greatly increased forward scattering.

Let us assume that the energy of the incident electron (k_i) is high enough so that we may neglect the energy differences $\epsilon_n - \epsilon_0$ in Eq. (3). In this case we can immediately sum over intermediate states in the matrix element and obtain an expression of the form

$$f^{(2)}(\eta) = \frac{2}{\pi^2} \int \frac{d^3q}{q^2 |\vec{q} - \vec{\eta}|^2} \times \frac{M_0(\eta) - M_0(q) M_0^*(\vec{q} - \vec{\eta})}{q^2 + 2\vec{q}\cdot\vec{k}_i - i\delta} . \tag{5}$$

For forward scattering, i.e., η small, the amplitude is divergent and the crucial region of the q integration is for small q as well. To leading order we may set $\eta = 0$ in the intergrand and use η as a lower cutoff on the limits of integration. In this case the scattering amplitude is well repre-

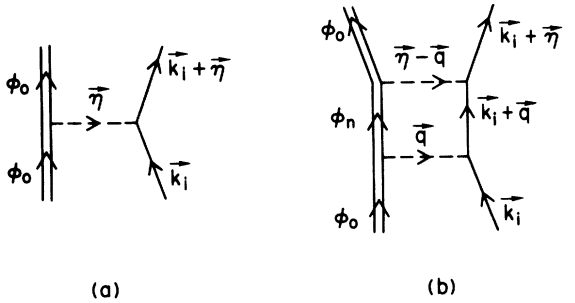

FIG. 1. Scattering of an electron by an atom. (a) The atom remains in its ground state and the scattering is the same as that of a static potential. (b) The atom is virtually excited to an intermediate state ϕ_n. The dashed line denotes the Coulomb interaction.

sented by

$$f^2(\eta) = \frac{4}{\pi}\int_{\eta}^{1} dq \int_{-1}^{1} d\mu \frac{\langle 0 | (\hat{q}\cdot\vec{r})^2 | 0\rangle}{q^2 + 2qk_i\mu - i\delta}$$

$$\simeq \frac{2id^2}{k_i}\ln(\eta)\,, \tag{6}$$

where $d^2 = \langle 0 | (\hat{q}\cdot\vec{r})^2 | 0\rangle$, is roughly the size of the ground-state wave function.

The logarithmic divergence in Eq. (6), at small η, is characteristic of a large small-angle scattering. Such a logarithmic divergence could have been obtained by simply Fourier transforming a complex potential of the form $V(r) \sim i/r^3$. In physical terms the electron excites the atomic system giving rise to a virtual dipole moment which then scatters the electron to its final state. On purely classical grounds we might expect the induced polarization potential to fall of as $1/r^4$. The quantum effect discussed above shows that the leading term is a purely imaginary i/r^3 potential. It is important to point out that this divergence is a direct consequence of our neglect of $\epsilon_n - \epsilon_0$ and is eliminated in a more accurate treatment of the problem. However, it is clear that a large enhancement of the forward scattering remains.

The second Born-approximation amplitude gives us a qualitatively accurate characterization of the inelastic processes. It is also true that an expression like Eq. (3) with minor modifications should qualitatively characterize the inelastic processes in solids associated with localized electrons. The corresponding perturbation diagrams are shown in Fig. 2. Here the double line represents a localized hole. The contribution to the scattering amplitude is again given by Eq. (3). There is actually an additional diagram which represents the same order process as shown in Fig. 2(b). It corresponds to exchanging the incident electron and the excited electrons. Such an exchange diagram involves large momentum transfer and will be negligible near the forward direction. We shall ignore these exchange diagrams in the present work, and evaluate Eq. (3) in some detail for copper metal taking into account the precise nature of the localized electronic wave functions and the screening of the Coulomb interaction by the conduction electrons. Having evaluated the amplitude we will then find the local complex energy-dependent potential $V^{(2)}(r)$ which reproduces this scattering in the lowest Born approximation, i.e.,

$$f^{(2)}(\eta) = \frac{1}{2\pi}\int d^3r\, e^{i\vec{q}\cdot\vec{r}} V^{(2)}(\vec{r})\,. \tag{7}$$

We will then utilize $V^{(2)}(\vec{r})$ obtained by inverting Eq. (7) in a Schrödinger equation of the form

$$[-\tfrac{1}{2}\nabla^2 + V^{(1)}(r) + V^{(2)}(r) - V^{ex}]\psi = E\psi \tag{8}$$

to calculate phase shifts, angular distributions, etc. In Eq. (8) $V^{(1)}$ is the Hartree potential and V^{ex} is the conventional nonlocal exchange potential, i.e.,[11]

$$V^{ex}\psi = \sum_{l,s}\int d^3r' \frac{1}{|\vec{r} - \vec{r}'|}\varphi^*_{ls}(\vec{r}')\psi(\vec{r}')\varphi_{ls}(\vec{r})\,. \tag{9}$$

Here the sum over l, s is over occupied electronic states. Solution of the Schrödinger equation is then equivalent to iteration of the Hartree-Fock scattering with the scattering depicted in Fig. 2(b).

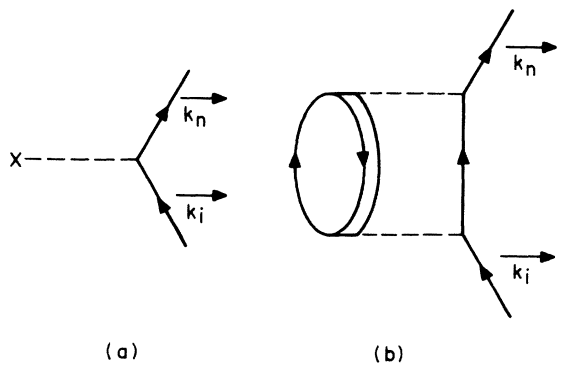

FIG. 2. (a) Scattering of an electron by the static potential of the atom. (b) The virtual excitation of a core state, denoted by the double line, to the continuum.

III. POLARIZATION PROCESSES IN COPPER

In order to evaluate Eq. (3) for copper metal we need to specify the nature of the transitions involved, evaluate the matrix elements in some approximate fashion, and take into account the screening of the other conduction electrons.

Since we are primarily interested in the complex character of the potential we need to determine which absorptive processes are dominant. The outer electrons, 4s in character, are rather uniform in space and lead to the usual uniform plasmon damping, i.e., they do not contribute to diffraction effects. The 3s, 3p, and 3d electrons are localized and there virtual excitation may be important. Optical-absorption data[12] which can be analyzed in terms of matrix elements similar to those shown in Eq. (3) (dipole only) indicate that absorption from these d electrons begins roughly at 10 eV and that the entire oscillator strength is used up by about 400 eV. The 3s and 3p electrons begin to contribute to the optical absorption at

about 100 eV and the absorptions extends to about 1000 eV. When electrons in the few-100-eV range scatter from such atoms we expect that the absorptive processes associated with the promotion of the d electrons is the dominant process. We will consider in some detail the contribution these processes make to the second-order Born amplitude.

Since the $3d$ electrons are rather well localized we choose the following spherical approximation to the atomic wave function[12] to represent the initial electronic state:

$$\varphi(r) = (4\pi)^{-1/2}(196\, e^{-8.05r} + 21.5\, e^{-3.5r} + 0.51\, e^{-1.55r}) . \tag{10}$$

For the excited states we use a plane wave with momentum k_n which is orthogonalized with respect to φ_0, i.e.,

$$\varphi_n(\vec{r}) = e^{i\vec{k}_n\cdot\vec{r}} - \varphi_0(\vec{r}) \int d^3r'\, \varphi_0^*(\vec{r}')e^{i\vec{k}_n\cdot\vec{r}'} . \tag{11}$$

The orthogonalization is necessary to reproduce the dipole matrix element $M_n(\vec{q}) \propto q$ in the small-q limit. Indeed in that limit our matrix element reduces to that used by Beaglehole[12] who showed that the wave function given by Eq. (10) is adequate to describe the optical absorption in Cu. The effective number of electrons per atom $n(\omega)$ available for optical absorption up to frequency ω is found to saturate at about 400 eV above threshold indicating that the oscillator strength is spread out over a large energy range because of the localized nature of the wave function.

To make further progress in evaluating Eq. (3) we divide up the q integration replacing the integrand with two different approximate forms in the region $q<\eta$ and $\eta<q$. In the second range we replace $|\vec{q}-\vec{\eta}|^2$ by q^2 and $M(\vec{q}-\vec{\eta})$ by $M(\vec{q})$. The angular average over $\vec{k}_n$ can then be performed for $|M(\vec{q})|^2$, i.e.,

$$[\bar{M}_n(q,\epsilon_n)]^2 = \langle\langle |M_n(\vec{q})|^2 \rangle\rangle \equiv \int |M_n(\vec{q})|^2 \frac{d\Omega_{k_n}}{4\pi} . \tag{12}$$

In the first range we replace $|\vec{q}-\vec{\eta}|^2$ by η^2 and $M_n(\vec{q}-\vec{\eta})$ by $M_n(-\vec{\eta})$. The angular average over $\vec{k}_n$ of $M_n(\vec{q})$ is slightly more difficult. We set

$$\langle\langle M_n(-\vec{\eta})M_n^*(\vec{q})\rangle\rangle \cong (q/\eta)\bar{M}_n(\eta)\bar{M}_n(q) . \tag{13}$$

The q/η factor comes into our approximate expression Eq. (13) because we want the matrix element to be accurate for small q and η, i.e., values of q and η small compared to the momentum which characterizes the localized d states. It is the small-q, small-η region, as we have seen [see Eq. (5)], which leads to the large forward scattering amplitude. In this limit and for $q \ll \eta$ it is easy to show that

$$\langle\langle M^*(\vec{q})M(\vec{q}-\vec{\eta})\rangle\rangle \sim q^2 , \tag{14}$$

whereas $\bar{M}(\vec{q})\bar{M}(\vec{\eta}) \sim q\eta$, hence the extra q/η.

We next discuss the question of screening. The Coulomb interaction between the electron and the polarization of the atom is screened by the metallic electrons. However, we are dealing with incident electrons with kinetic energy much larger than the Fermi energy so that the screening must be considered dynamic with characteristic frequency

$$2\omega = k_i^2 - (\vec{k}_i - \vec{q})^2 \approx 2\vec{k}_i\cdot\vec{q} . \tag{15}$$

If ω is much greater than the plasma frequency, the Coulomb interaction is unscreened. In the present case the frequency is proportional to q. The dielectric function for a fixed ratio $x \equiv (\omega/E_F)/(q/k_f)$, and $q \to 0$ is given by[13]

$$\epsilon(q, qx) = 1 + \lambda_{TF}^{-2} q^{-2}\left(1 - \frac{x}{2}\ln\left|\frac{1+x}{1-x}\right|\right) . \tag{16}$$

We see that when $x=0$ we get the static screening with the Thomas-Fermi screening length λ_{TF}. As x increases the term in parentheses in Eq. (16) becomes less than unity and we have effectively a longer screening length. For $x>1$ the term in parentheses becomes negative and we get into the dynamic overscreening regime. For our present problem $\omega = \vec{k}_i\cdot\vec{q}$ and depending on the angle between $\vec{k}_i$ and $\vec{q}$ the ratio x can be greater than or less than unity. If we examine in detail how the dielectric function $\epsilon(q, \vec{k}_i\cdot\vec{q})$ screens a point charge,[14] we conclude that the effective potential can be approximated by a screened potential with a screening length which is reduced from the static Fermi-Thomas screening length λ_{TF} by a factor proportional to the electron velocity, i.e., $\lambda = \lambda_{TF} k_F/k_i$. This is the approximation we shall adopt here.

The expression for $f^{(2)}(\eta)$ then simplifies to

$$f^{(2)}(\eta) = \frac{20}{\pi^3}\int k_n^2 dk_n [1 - f(\epsilon_n)] \int_{-1}^{+1} dx \left(\int_0^{\eta} dq \frac{q^3 \bar{M}(q,\epsilon_n)\bar{M}(\eta,\epsilon_n)}{\eta(\eta^2+\lambda^2)(q^2+\lambda^2)[q^2 + 2(\epsilon_n - \epsilon_0) + 2qk_i x - i\delta]} + \int_{\eta}^{\infty} dq \frac{q^2}{(q^2+\lambda^2)^2} \frac{\bar{M}(q,\epsilon_n)^2}{[q^2 + 2(\epsilon_n - \epsilon_0) + 2qk_i x - i\delta]} \right) , \tag{17}$$

where we have inserted a factor of 10 to account for the 10 occupied d electrons. The factor $f(\epsilon_n)$ is the usual Fermi factor, and we have ignored the process in which the intermediate state is a hole state in the Fermi sea, as this process involves large energy denominator for incident energies large compared with the Fermi energy. The x integral in Eq. (17) is easily done and the resulting two-dimensional integral has been evaluated numerically.

The results of this numerical procedure are shown in Figs. 3–6. The complex potential $V^{(2)}(r)$ is attractive with a magnitude of several atomic units and a range of approximately 1 a.u. It is also clear from these figures that the potential is quite energy dependent over an energy range of several hundred eV. It is of interest to compare the real part of the potential to the usual Hartree potential. At small distances $r = 0.25$ the Hartree potential is about 50 a.u. (about one order of magnitude larger then $\mathrm{Re}[V^{(2)}(r)]$). At $r = 0.5$ and 1 it has dropped to 12 and 1.4 a.u., respectively, and by $r = 2$ it is down to 0.3 a.u.

In Fig. 7 and Table I we show the appropriate phase shifts obtained from a numerical solution of the Schrödinger equation, and in Fig. 8 we have plotted the angular distribution of electrons scattered from a single Cu atom in the host metal. In both cases the HF and HFS results are shown for comparison purposes.

In Fig. 8 the angular distribution calculated by including polarization effects shows the expected

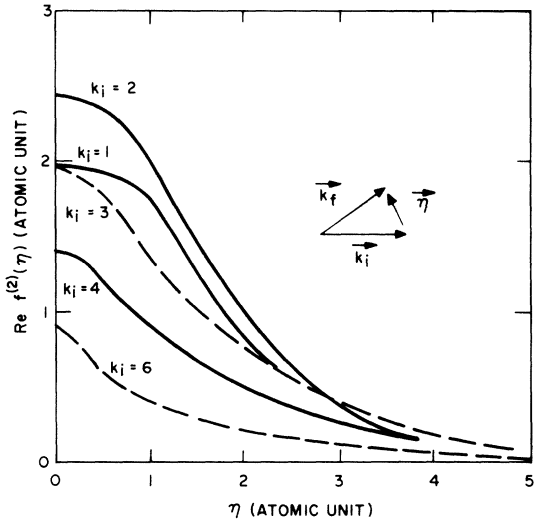

FIG. 3. Real part of the second Born scattering amplitude vs momentum transfer η for several incident momentum k_i. An energy-dependent screening of the Coulomb interaction as discussed in the text has been used in these calculations.

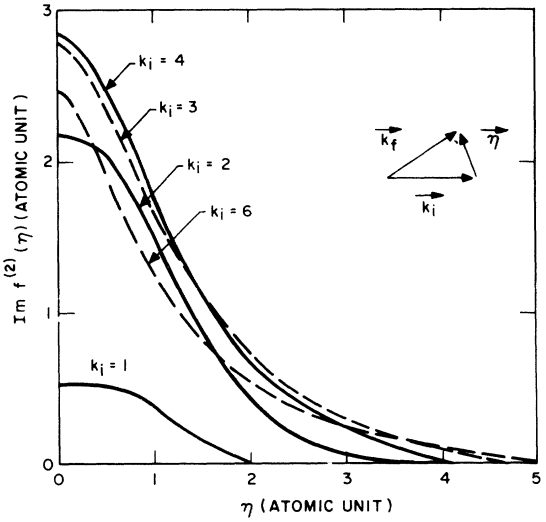

FIG. 4. Imaginary part of the second Born amplitude.

peak in the forward direction and the reduction in the back direction compared with the HF value. It is interesting to note that for both Figs. 7 and 8 at low to moderate energy HFS is numerically closer to the results of the present calculation. On the surface at least this seems to indicate that the Slater $\rho^{1/3}$ exchange is doing a good job of imitating the exchange plus correlation, i.e., the second-order polarization process as computed here. However, the HFS phase shifts deviate systematically at higher energy from both the HF and the present calculation. This is because an energy-independent exchange and correlation has been used in HFS, whereas in HF the exchange part of the potential is reducing with increasing energy. In our present calculation, the correlation part is also being reduced. In LEED calculations the turning off of the exchange and correlation energy

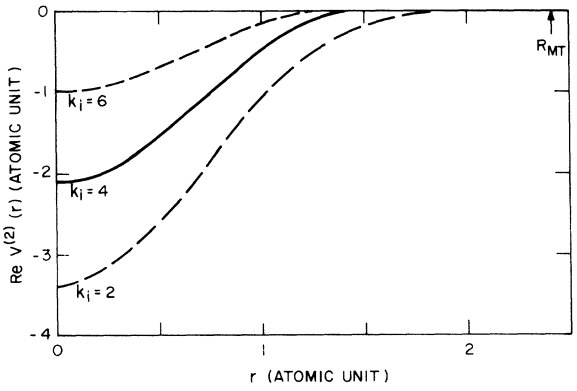

FIG. 5. Real part of the optical potential $V^{(2)}(r)$.

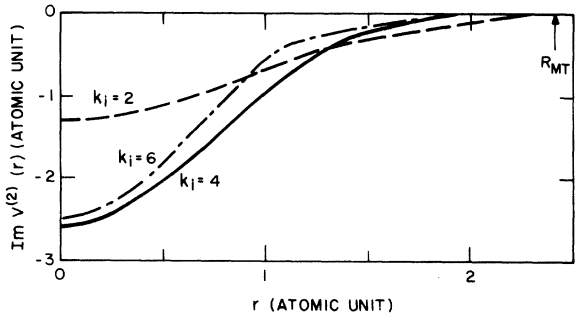

FIG. 6. Imaginary part of the optical potential $V^{(2)}(r)$.

is partially accounted for by introducing a phenomenological inner potential which sets the zero of energy in the crystal and is energy dependent.[5] Our results here show that both the real and imaginary part of the correlation potentials vary both in space and with energy and should not be approximated by constant inner potentials.

In order to see if the size of the potential computed here is generally consistent with known experimental data we have looked at its contribution to the imaginary part of the self-energy of an electron. The imaginary part of the self-energy Σ is obtained from

$$\mathrm{Im}\Sigma = 2\pi N_I \mathrm{Im} f^{(2)}(0) . \tag{18}$$

Here N_I is the ion density. In Fig. 9 $\mathrm{Im}\Sigma$ is plotted as a function of the incident momentum for both screened and unscreened cases. This provides us with a good estimate of the over-all importance of screening. The magnitudes of $\mathrm{Im}\Sigma$ for the screened case is roughly 6 eV and relatively independent of the electron energy beyond threshold. The imaginary potential deduced for LEED experiments is about 4 eV. However, these two numbers may not be directly comparable as the LEED value is obtained by analyzing the data using a constant complex inner potential. Our value of 6 eV may be considered to be of the correct order of magnitude.

While the $\mathrm{Im}f^{(2)}(0)$ is of the correct order of magnitude our approximate evaluation of Eq. (17) for $f^{(2)}(\eta)$ is less accurate for large momentum transfer. This in turn means that we are less confident about the accuracy of $V^{(2)}(r)$ for small r. Such inaccuracy might lead to errors in the imaginary part of the phase shifts and in $f(\theta)$. The imaginary part of δ is rather large especially for $l = 3$ or 4 and may reflect this uncertainty.

IV. APPLICATION TO EXAFS

The potentials derived in Sec. III may be applied to a variety of problems including LEED, band

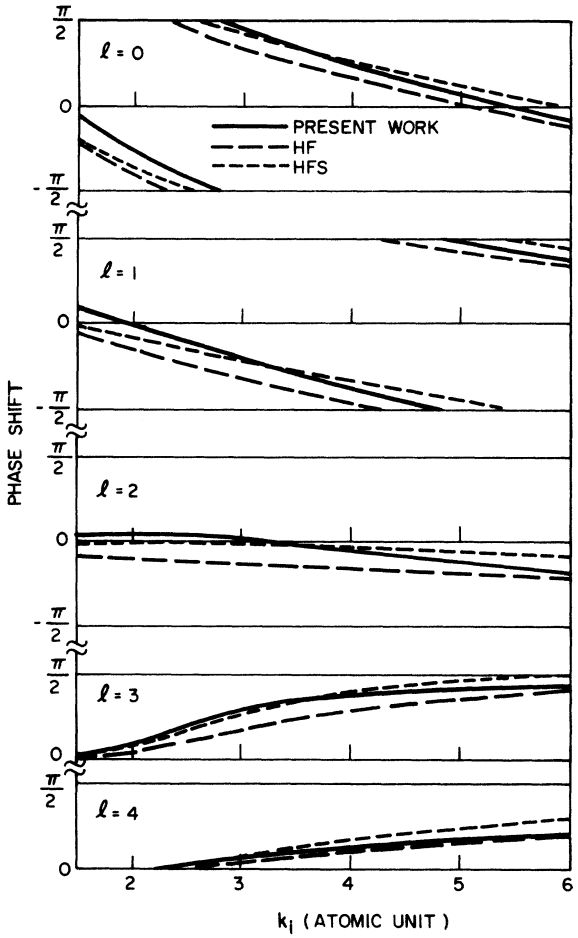

FIG. 7. Phase shifts for copper vs electron momentum calculated in the Hartree-Fock and the Hartree-Fock-Slater approximations and including polarization effects in the present work. In all cases the atomic wave functions are truncated at the muffin-tin radius and normalized within the muffin tin sphere to preserve charge neutrality. The zero of energy is taken at the muffin-tin zero which is the vacuum level for HF and for the present calculation but is several eV below the vacuum level in HFS.

structure, and EXAFS. We will, for the purposes of illustration, focus on the EXAFS problem in copper and even more specifically analyze the role such effects play in two problems: (i) the so-called fourth-shell anomaly, and (ii) the k dependence of the central-atom phase shift.

EXAFS refers to the modulation of the absorption coefficient $\chi(k)$. For K-shell excitation this modulation is describable by the following simple expression:

$$\chi(k) = -\sum_i \frac{\mathrm{Im}[f(\pi)e^{2ikr_i+2i\delta_i}]e^{-2\gamma r_i}}{kr_i^2} . \tag{19}$$

TABLE I. Complex phase shift for copper.

	l \ k_i	1	2	3	4	5	6
Reδ_l	0	0.41	−0.84	1.43	0.74	0.21	−0.22
Imδ_l		(0.086)	(0.28)	(0.35)	(0.30)	(0.26)	(0.20)
	1	0.45	0.03	−0.63	−1.18	1.52	1.18
		(0.13)	(0.34)	(0.38)	(0.33)	(0.29)	(0.22)
	2	0.01	0.17	0.073	−0.16	2.78	−0.52
		(0.02)	(0.34)	(0.45)	(0.41)	(0.36)	(0.27)
	3	0.01	0.29	0.92	1.25	1.33	1.39
		(0.003)	(0.44)	(0.81)	(0.54)	(0.40)	(0.28)
	4	0.0004	0.043	0.21	0.40	0.57	0.71
		(0.0001)	(0.038)	(0.18)	(0.25)	(0.24)	(0.21)
	5		0.006	0.07	0.15	0.27	0.38
			(0.006)	(0.06)	(0.09)	(0.13)	(0.14)
	6			0.021	0.073	0.14	0.21
				(0.02)	(0.05)	(0.07)	(0.08)
	7				0.04	0.077	0.12
					(0.03)	(0.047)	(0.06)
	8				0.013	0.036	0.067
					(0.014)	(0.033)	(0.04)
	9					0.018	0.041
						(0.022)	(0.03)

Here $k=[2m(\omega-\Omega_{\text{th}})]^{1/2}$ is the wave vector of the free electron promoted above threshold Ω_{th} to the continuum from the K shell by a photon of frequency ω. Equation (19) describes the modification of the final state as the photoelectron propagates outwards and is backscattered by the ith atom located a distance r_i away and then propagates back towards the origin. The spherical outgoing wave has been approximated by a plane wave and $f_i(\pi)$ is the backscattering amplitude. The phase shift δ_l' describes the effect of the potential of the excited atom. The damping factor γ takes into account inelastic scattering of the photoelectron.

Up to now inelastic losses have been approximated by adding an imaginary potential which is assumed to be constant (~4 eV) throughout the crystal. This implies, for $\gamma \ll k$, that $\gamma = 0.147/k$ in atomic units. While such an approximation may be adequate for inelastic scattering due to plasmon excitation, we have learned that the complex potential is in fact nonuniform, when the excitation of more localized states like the d states is in-

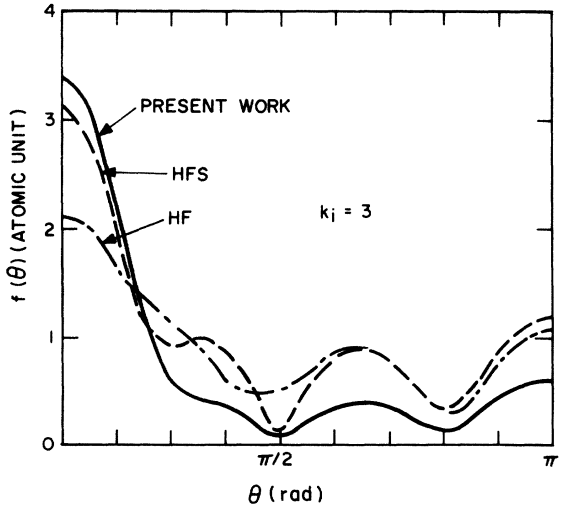

FIG. 8. Scattering amplitude for $k_i = 3$ a.u. calculated in the Hartree-Fock and Hartree-Fock-Slater approximations and including polarization effects.

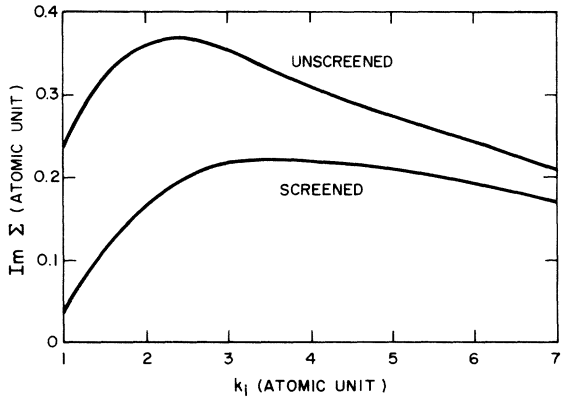

FIG. 9. Imaginary part of the electron self-energy due to d-band excitation in copper metal calculated by using either an unscreened Coulomb interaction, or by using an energy-dependent screening length as discussed in the text.

cluded.

Let us first consider backscattering from a nearest neighbor. In a more accurate treatment which includes the nonuniform complex potential one should use a smaller γ to describe plasmon losses only and one should calculate $f(\pi)$ with complex phase shifts. As we can see from Fig. 8 $f(\pi)$ calculated this way is reduced from the Hartree-Fock or Hartree-Fock-Slater approximation. In addition one should use a complex δ_1' to describe inelastic losses in the central atom. This kind of treatment for neighbors that are further apart will in general be quite difficult as one must consider losses due to excitation of other atoms in between.

A particularly interesting application of some of these ideas is to a calculation of the fourth-shell contribution to EXAFS in fcc metals such as copper. A fourth-shell atom is directly shadowed by a first-shell atom and its shell radius r_4 is $2r_1$, where r_1 is the first-shell radius. It has been pointed out[2] that scattering by the first-shell atom greatly influences the EXAFS contribution of the fourth shell. Again, approximating spherical waves with plane waves we can write down the following equation for the fourth-shell contribution to χ: i.e.,

$$\chi_4(k) = -\frac{N_4}{k}\mathrm{Im}\left[f(\pi)\left(\frac{1}{r_4^2}+\frac{2f(0)}{r_1}\frac{1}{r_1}\frac{1}{r_4}+\frac{f^2(0)}{r_1^4}\right)\times e^{i2kr_4+2i\delta_1'}\right]e^{-2\gamma r_4}, \tag{20}$$

where N_4 is the number of atoms in the fourth shell. The second term describes the forward scattering by the first-shell atom on either the outward or the return trip of the photoelectron and the third term describes forward scattering on both trips. The factors of r_1^{-1} arise from the strength of the various spherical waves. The first term describes only a single backscattering and we denote its contribution by $\chi_4^{(0)}$.

Using the HF phase shifts and a constant imaginary potential, we obtain at $k=3$

$$\chi_4^{\mathrm{HF}} = 2.5e^{i\pi/3}\chi_4^{(0)}. \tag{21}$$

Experimentally it has been found that the fourth-shell contribution is roughly π radians out of phase with the other shells and its magnitude is three or four times larger than given by $\chi_4^{(0)}$. (The precise discrepancy in the magnitude is difficult to ascertain as it depends on the assumed magnitude of γ.) Thus Eq. (21) while qualitatively correcting things in the right direction, is still insufficient to explain the experiment.

Equation (21) is based on the assumption of a uniform imaginary potential. We have seen that a nonuniform imaginary potential has the effect of enhancing the forward scattering amplitude rather than reducing it as has been done in Eq. (20) by assuming that $e^{-2\gamma r_4}$ multiplies the multiple as well as single scattering amplitudes. To illustrate this point let us make the following crude estimate. We treat the inelastic loss in the central atom and in the fourth-shell atom by a damping factor as before which requires a factor of $e^{-2\gamma r_1}$. For the sake of illustration we assume that all the damping is due to d-electron excitation. Then instead of a factor $e^{-2\gamma r_1}$ to account for damping while traversing the first-shell atom, we should use $f'(0)$ computed using complex phase shifts. This results in the equation

$$\chi_4 = \left(1+\frac{8f'(0)}{r_4}+\frac{16f'^2(0)}{r_4^2}\right)e^{+2\gamma r_1}\chi_4^{(0)}, \tag{22}$$

where $\gamma = 0.147/k$ is the same damping coefficient used in arriving at Eq. (21). If $k=3$, we obtain

$$\chi_4 \approx 5.13e^{i\pi/2}\chi_4^{(0)}, \tag{23}$$

approximately twice as big as the value given in Eq. (16) and with a phase shift of $\frac{1}{2}\pi$. The assumption of d-electron damping clearly leads to an overestimation but Eq. (23) indicates that the fourth-shell contribution to EXAFS can be greatly enhanced, due to the increased forward scattering amplitude which explicitly arises from the nonuniform absorption computed here. Such effects seem to be in the correct direction to explain the observed discrepancy between theory and experiment.

A second problem related to EXAFS is the k dependence of the central-atom phase shift $\delta_1'(k)$. As we can see from Fig. 7, $\delta_1'(k)$ is quite linear in k. From Eq. (14) we see that the linear dependence of $\delta_1'(k)$ gives rise to an effective shift in the radial distances and thus it is important for absolute distance determination. It has been found[1,2] that in Cu the slope calculated using the HF potential is too small by about 30% when compared with experiment. As pointed out earlier the present calculation produces an $l=1$ phase shift that has a steeper slope than the HF approximation. This is a general feature of such calculations since the polarization part of the potential weakens as the energy increases. Thus it is hopeful that the inclusion of polarization effects will lead to an accurate calculation of the central-atom phase shift. Further work on this particular problem is in progress.

V. CONCLUSION

We have shown that polarization effects are important in electron-atom scattering even inside a solid. By considering the example of the excitation of d states in copper we explicitly construct a com-

plex optical potential which has spatial variation. The usual approximation of a spatially uniform complex inner potential is thus not valid. The localized nature of the optical potential has a particularly dramatic effect on the scattering amplitude in the forward direction and has interesting implications for the fourth-shell anomaly in EXAFS. While we have not explicitly discussed the implications for LEED calculation, it will clearly be of interest to perform LEED calculations using such complex energy-dependent potentials.

---

[1]E. A. Stern, Phys. Rev. B 10, 3027 (1974).
[2]P. A. Lee and J. B. Pendry, Phys. Rev. B 11, 2795 (1975).
[3]C. A. Ashley and S. Doniach, Phys. Rev. B 11, 1279 (1975).
[4]J. B. Pendry, *Low Energy Electron Diffraction* (Academic, New York, 1974).
[5]D. W. Jepsen, P. M. Marcus, and F. Jona, Phys. Rev. B 5, 3933 (1972).
[6]J. B. Pendry, J. Phys. C 4, 2501 (1971); 5, 7567 (1972); the program is listed in J. B. Pendry, *Low Energy Electron Diffraction* (Academic, New York, 1974).
[7]There have been two recent preliminary attempts to access the accuracy of this approximation: G. Beni, P. A. Lee, and P. M. Platzman, Bull. Am. Phys. Soc. 20, 488 (1975); and B. S. Ing and J. B. Pendry, J. Phys. C 8, 1087 (1975). There have also been previous evaluations of the second Born scattering amplitude in solids for electrons in the 100-keV range by H. Yoshioka, J. Phys. Soc. Jpn. 12, 618 (1957); and M. J. Whelan, J. Appl. Phys. 36, 2099 (1965).
[8]L. I. Shiff, *Quantum Mechanics* (McGraw-Hill, New York, 1955).
[9]W. Williams and S. Trajmar, Phys. Rev. Lett. 33, 187 (1974).
[10]H. S. Massey and C. B. O. Mohr, Proc. R. Soc. A 195, 880 (1934).
[11]C. Kittel, *Quantum Theory of Solids* (Wiley, New York, 1964).
[12]A. Beaglehole, Proc. Phys. Soc. Lond. 87, 461 (1966). In this reference the correct angular dependence of the d-wave function is included. In the present work we have taken a spherical average of the wave function for simplicity. The result for the effective number of electrons $n(\omega)$ compares well with that of Beaglehole indicating that this approximation is justified.
[13]A. L. Fetter and J. D. Walecka, *Quantum Theory of Many-Particle Systems* (McGraw-Hill, New York, 1971), p. 163.
[14]P. A. Lee (unpublished).